2021 IEEE 22nd International Symposium on a World of Wireless, Mobile and Multimedia Networks (WoWMoM) | 978-1-6654-2263-5/20/$31.00 ©2021 IEEE | DOI: 10.1109/WoWMoM51794.2021.00055

Effect of Antenna Orientation on the Air-to-Air Channel in Arbitrary 3D Space

N. Cameron Matson, Syed Muhammad Hashir, Sicheng Song, Dinesh Rajan, and Joseph Camp
Department of Electrical and Computer Engineering, Southern Methodist University, Dallas, TX, USA
Email: {cmatson, hashirs, songs, rajand, camp}@smu.edu

***Abstract*—Unmanned Aerial Vehicles (UAVs) often lack the size, weight, and power to support large antenna arrays or a large number of radio chains. Despite such limitations, emerging applications that require the use of swarms, where UAVs form a pattern and coordinate towards a common goal, must have the capability to transmit in any direction in three-dimensional (3D) space from moment to moment. In this work, we design a measurement study to evaluate the role of antenna polarization diversity on UAV systems communicating in arbitrary 3D space. To do so, we construct flight patterns where one transmitting UAV is hovering at a high altitude (80 m) and a receiving UAV hovers at 114 different positions that span 3D space at a radial distance of approximately 20 m along equally-spaced elevation and azimuth angles. To understand the role of diverse antenna polarizations, both UAVs have a horizontally-mounted antenna and a vertically-mounted antenna—each attached to a dedicated radio chain—creating four wireless channels. With this measurement campaign, we seek to understand how to optimally select an antenna orientation and quantify the gains in such selections.**

***Index Terms*—A2A channel, unmanned aerial vehicles, wireless channel measurements, antenna polarization**

I. Introduction

The next wave of UAV applications requires concurrent operation and coordination of drone platforms to achieve tasks such as emergency relief, search and rescue, and autonomous defense [1]. Inherently in such situations, UAV platforms must be able to communicate at any moment in three-dimensional (3D) space to peer drones, fixed infrastructure, or vehicles on the ground. Achieving this 3D communication is a challenge, as UAVs have limited size, weight, and power, precluding large antenna arrays or many radio chains that could be used to send across the full range of azimuth and elevation angles.

A number of prior works have simulated drone networks, often focusing on the flight dynamics and modeling with simplifying assumptions for UAV connectivity [2], [3]. There have been a number of recent UAV channel measurement studies; see the surveys [4], [5]. These works represent a wide variety of UAV experiments (different types of aircraft, varying degrees of mobility, and multiple environments,) but of the majority of these works, e.g. [6]–[17] consider only the air-to-ground (A2G) channel. In each of the studies, the authors investigate how some of the unique aspects of communication systems involving UAVs affect the wireless channel. For example, some [6], [7] investigate the effect of airframe shadowing on the channel. Others [8]–[11] observe the impact of the relative elevation angle between the UAV and the ground station. The type of antenna used and how it is mounted on the UAV can be a determining factor in how much the airframe or elevation angle affects the channel. Multiple antenna orientations are explored in [12]–[17].

Likely because of the inherent challenges of controlling multiple UAV platforms in flight, there have been far fewer campaigns to measure the air-to-air (A2A) channel [16]–[20]. These studies have either involved small aerial sensors [17]–[19], or only considered a limited number of angles in 3D space [16], [20]. Our previous work [21], [22] has investigated the effect of antenna orientation and placement on the A2A wireless channel for a limited number of azimuth and elevation angles.

In this work, we design a measurement study to evaluate the role of antenna polarization diversity on UAV systems communicating in arbitrary 3D space. To focus on the role of the diverse characteristics of drone communication systems and their corresponding impact on A2A links, we hover a transmitting drone at a high-altitude (80 m) to ensure line of sight wireless channels and minimal multipath reflections from obstacles in the environment. Then, we hover a receiving drone at 114 unique locations that span 3D space at a radial distance of approximately 20 m with 22.5 degree separation between azimuth and elevation angles The transmitter and receiver each have two radio chains equipped with vertical and horizontally mounted antennas. We use two distinct tones on the same carrier frequency on an isolated 2.4 GHz channel to distinguish between four simultaneous single-input, single-output (SISO) channels. We then compare these channels to quantify their impact of antenna orientation for various azimuth and elevation angles.

The main contributions of this paper are as follows:

- We design a robust drone-to-drone 2x2 channel measurement system covering 114 uniformly spaced azimuth and elevation angles in 3D space. The system is outfitted with GPS and inertial measurement unit sensors to allow for accurate and precise control.
- We compute the throughput of four transmitter-receiver pairs of vertically and horizontally oriented antennas. We observe that each of the four pairs experiences deep fades at different sets of angles. This suggests that a strategy of dynamically selecting the antenna orientations based on relative position would result in consistent throughput in arbitrary 3D space.

978-1-6654-2263-5/21/$31.00 ©2021 IEEE
DOI 10.1109/WoWMoM51794.2021.00055

This paper is organized as follows. We present the design of both our flight plan and measurement platform and discuss the alignment of the UAV flight data with the wireless channel measurements in Section II. The system model is introduced in III. In Section IV, we evaluate the accuracy of the UAV flight plans. In Section V, we experimentally evaluate the capacity of different transmit-receive antenna orientation pairs, and we conclude in Section VI.

II. Measurement Campaign and Challenges

In this section, we describe the design of the flight plan and the implementation of a flyable 2x2 channel sounding system.

A. 3D Space and Flight Plan Design

We use a spherical coordinate system shown in Fig. 1a to describe the position of the receiver and transmitter drones. The location of the transmit drone, which hovers 80 m above the ground, is defined as the origin. In our experiment, the receiver drone hovers at fixed locations around the transmitter in 3D space at a radial distance of roughly 20 m. These locations are defined by an angle pair (ϕ, θ). The azimuth angle, ϕ, is measured clockwise from the West axis and varies between 0° and 360°. The elevation angle, θ, is defined as the angle above or below parallel (both drones at same height) and varies between -90° (receiver is directly below the transmitter) and 90° (receiver is directly above the transmitter). We take measurements over 16 azimuth and nine elevation angles at intervals of 22.5° for a total of 114 unique locations spanning 3D space (Note that at locations directly above or below, $\theta = \pm 90^\circ$, the azimuth angle ϕ is undefined).

To reliably control the position of the receiver drone, the spherical coordinates (ϕ, θ) are translated into GPS coordinates (longitude, latitude, elevation) using the MATLAB Mapping Toolbox, exported to a keyhole-markup-language (.kml) file, and uploaded to the DJI GSPro flight planner tool. Flight time is limited by the capacity of the drone battery; therefore, measurements are taken over eight flights consisting of 16 locations each. During each flight, the receiver begins at $\theta = 0^\circ$ and flies in a vertical circle around the transmitter, hovering for 20 seconds at each elevation angle. Both UAVs always face North during the experiment.

B. Programmable Drone-Based 2x2 Channel Sounding System

For our wireless measurements, we implement a 2x2 channel sounding system using two Universal Software Radio Peripheral (USRP) E312 from Ettus research. The USRP E312 has two RF transceivers, which are clocked from the same local oscillator. This SDR is also equipped with Inertial Measurement Unit (IMU) to capture orientation information. We utilize GNU Radio and USRP Hardware Driver (UHD) libraries in Python to transmit and receive In-Phase and Quadrature (IQ) samples.

1) Transmitter: During the experiment, the transmitter generates two complex, sinusoidal tones–one at 5 kHz (f_1) and another at 15 kHz (f_2). These tones are independently transmitted from channels TRXA and TRXB, respectively, of the E312 over a 2.484 GHz carrier frequency for an isolated channel free from interference. Each transmit channel is equipped with an omni-directional (VERT2450) antenna with 3 dBi gain. The TRXA antenna is mounted horizontally while the TRXB antenna is mounted vertically. We attach the transmitter on the top of the UAV using custom-made 3D-printed parts to secure the SDR and antennas and ensure robustness to in-flight vibrations (Fig. 1b).

2) Receiver: We mount the receiver (SDR and antennas) on the UAV in an identical manner to the transmitter. The transmitted tones are captured on the two different channels of the receiver E312 which are post-processed offline in MATLAB. The baseband signal on each channel is sampled at 200 kSamples/second. The receiver continuously records data for the duration of each flight. To aid with synchronization of the IQ data and UAV flight log, we record the start and stop time of the USRP script to calculate the time stamp of each received sample and the on-board IMU sensor data (*i.e.*, roll, pitch, and yaw) of the USRP.

C. Extracting Measurement Locations

1) Flight Log: The DJI GSPro flight planner tool records flight data such as speed, GPS coordinates, and IMU readings continuously, but the log does not indicate the waypoints from the flight plan; therefore, we need a method for identifying which samples correspond to each measurement location. To identify waypoint locations, we compute a simple metric $g_{UAV}(t)$ that captures the combined effect of the roll $r_{UAV}(t)$ and pitch $p_{UAV}(t)$ components of the IMU sensor as follows:

$$g_{UAV}(t) = \sqrt{r^2_{UAV}(t) + p^2_{UAV}(t)}. \tag{1}$$

We then perform peak-finding on g_{UAV}. We assume that at the midpoint in time between two peaks, the receiver is midway through its 20-second hover. From this timestamp, we isolate a 1-second window centered at the midpoint to analyze the receiver position.

2) USRP IQ Samples: In addition to the flight log timestamps, we also have the start and stop time of the IQ data recording. Unfortunately, because of the separate processors of the UAV and USRP, we have two notions of time, and thus need a method to align the two data sets. We do so by utilizing the IMU sensors of both the USRP and UAV. We compute $g_{USRP}(t)$ from $r_{USRP}(t)$ and $p_{USRP}(t)$ as in (1). We perform peak-finding on g_{USRP}. Then, to align the two IMU signals, we calculate the delay between the first peak in $g_{UAV}(t)$ (which corresponds to takeoff) and the nearest peak in $g_{USRP}(t)$ and apply this delay to the appropriate time signal.

We now have the same notion of time for the USRP and UAV signals, which along with the known sampling rates of each, allows us to match samples from the UAV flight log and the measured IQ data from the USRP. We repeat this process for each flight. Once the IQ samples have been matched to the corresponding azimuth and elevation angles of each measurement location, we analyze the individual

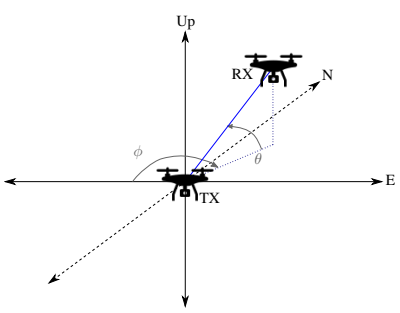

(a) Coordinate System

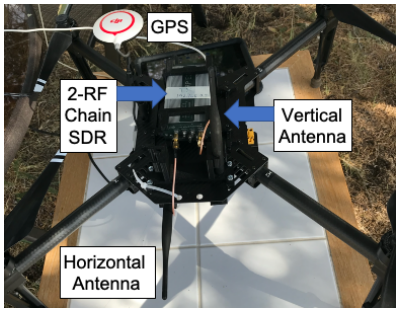

(b) UAV Communications Platform

Fig. 1: The spherical coordinate system used in the experiment (a). Both drones are always facing North. The SDR/antenna setup matched for TX/RX (b). Antennas are mounted on the front of each drone.

SISO channels (see Fig. 3) using the procedure described in Section III.

Fig. 2 shows $g_{USRP}(t)$, the envelope of the IQ data for one of the receiver channels for one flight, and the identified waypoints. The samples corresponding to the measurement waypoint are then saved for further processing.

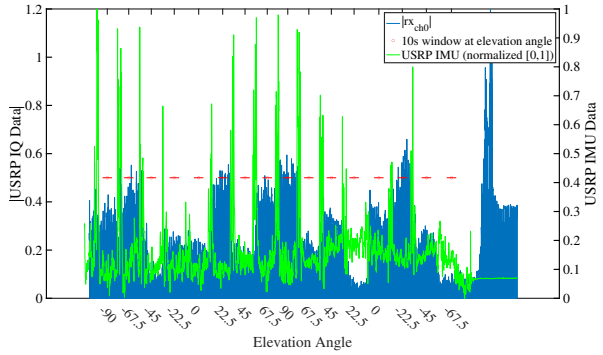

Fig. 2: Envelope of the one receiver antenna's IQ Data along with identified waypoints from IMU synchronization.

III. Wireless Performance Metric

In this section, we first present the wireless channel model of our measurement system and then describe the metric that we use to characterize the channel.

A. System Model

A simplified model for the measurement system is shown in Fig. 3. Let x_H and x_V represent the signals transmitted by the two RF chains at the TX USRP. Similarly, let y_H and y_V represent the signals received at the two RF chains at the RX USRP. The discrete-time received signal, $\mathbf{y}$, at time n at the two chains in the RX USRP can be written in matrix form as:

$$\mathbf{y}(n) = \mathbf{H}\mathbf{x}(n) + \mathbf{n}(n) \tag{2}$$

where $\mathbf{y}(n) = [y_H(n)\ y_V(n)]^T$, $\mathbf{x}(n) = [x_H(n)\ x_V(n)]^T$ and $\mathbf{n}(n) = [n_H(n)\ n_V(n)]^T$ represents the effective noise at the 2 receiver RF chains. The channel matrix $\mathbf{H} = \begin{bmatrix} h_{HH} & h_{HV} \\ h_{VH} & h_{VV} \end{bmatrix}$ represents the channel between the two transmit and two receive antennas. The subscripts V and H represent the vertical and horizontal polarizations of the antennas on the USRPs. For example, h_{VH} is the channel between the horizontal receive antenna and the vertical transmit antenna. In our experiments, we transmit a fixed complex sinusoid at different frequencies from the two transmit antennas. These tones allow us to estimate all four channels in $\mathbf{H}$ simultaneously. Specifically, we set $x_H(n) = 0.7e^{j2\pi f_1 n}$ and $x_V(n) = 0.7e^{j2\pi f_2 n}$ where f_1 and f_2 were selected as 5 kHz and 15 kHz, respectively, and n represents the time-index. To estimate the channel, we compute the least squares estimate $\hat{\mathbf{H}}$ of the channel using a finite number of signal samples:

$$\hat{\mathbf{H}} = (\mathbf{X^H X})^{-1}\mathbf{X^H Y}, \tag{3}$$

where $\mathbf{X}$ is two-by-N shaped matrix consisting of N consecutive, non-overlapping samples of the transmit signal, $\mathbf{Y}$ is a similarly shaped matrix of output samples, and $\mathbf{X^H}$ is the Hermitian or conjugate transpose of $\mathbf{X}$. For each of the N samples, a single estimate of the channel is obtained. We experimentally consider different values for N but only show the results for N=100 samples as it allows for low mean-squared-error over the segment without over-fitting. The entire processing of the RX USRP data to obtain the channel estimate is conducted in MATLAB.

B. Capacity Measure

We use capacity to quantify the quality of one of the four wireless channels in $\hat{\mathbf{H}}$. For example, the capacity per unit bandwidth of the channel h_{VV} can be calculated as [23]:

$$C_{VV} = \log_2(1 + \frac{P}{N_o}h_{VV}^2) \tag{4}$$

In (4), P/N_o is the signal (P) to noise (N_o) ratio (SNR) at the vertical receiver antenna element. For simplicity, we normalize by setting P=1 and measuring the effective noise power N_o at the receiver when there is no transmit signal. Similarly, we calculate the capacity of the h_{VH}, h_{HV} and h_{HH} channels using (4).

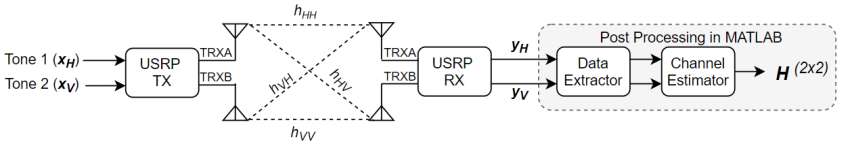

Fig. 3: 2x2 Channel Sounding System Model.

IV. Quantifying UAV Flight Plan Accuracy

We suspect one reason for the lack of in-field, air-to-air channel measurements is the difficulty of simultaneously flying multiple UAVs accurately and precisely. We have observed this in our previous work [22]. There are many variables such as GPS inaccuracies, wind, and drone vibrations within a single flying system, let alone two, especially over several flights. We would like to be able to control these variables as much as possible, but when we cannot control them completely, we would like to quantify them to observe their effects.

In this study, we seek to measure the channel at a receiver drone located at distinct azimuth and elevation angles from a transmitter drone. To this end, we quantify how accurately those azimuth and elevation angles are reproduced in the experiment. We the present absolute position of both the transmitter and receiver to demonstrate that their positions are stable when hovering. Then we discuss their relative position, i.e. the angular separation between the two drones, and show that our experiment uniformly samples locations over the 3D space around the transmitter.

1) Transmitter Position: Fig. 4a shows the transmit drone's average displacement (Δ) from the intended location based on the UAV GPS data for each of the eight flights. There is a small variation in the mean positions between the flights; however, since the variation is less than a meter, the mean positions can be treated effectively the same. Further, the standard deviation within each flight suggests how much the transmitter drone moved as it hovered in place. The average deviation in the displacement across all flights was only 80 mm, which indicates that the transmitter was effectively stationary.

2) Receiver Position: For the receiver, we partition each flight log in a similar manner as the one described in Section II-C2. This way our waypoint location data closely matches in time to our wireless measurements. As with the transmitter, we want to ensure that the receiver UAV is close to its intended location and is stable at that location for each waypoint along the flight. As an example, consider Fig. 4b, which shows the average displacement from the intended location for each elevation angle when the azimuth angle was equal to 0. While the average displacement of the receiver is higher than that of the transmitter, it is relatively small compared to the separation distance between the transmitter and receiver of 20 m. Again, what is more important is the standard deviation. Across all measurement locations, the average standard deviation of displacement from the intended receiver location was 161 mm suggesting that the receiver's position was fixed.

We have shown that the transmitter and receiver are effectively stationary at each of the measurement locations; however, there are some absolute position errors. A reasonable question is whether or not those errors affect the ability of the study to capture the A2A channel over all angles in 3D space. As it turns out, the positional errors are small enough relative to the drone separation distance that each of the (ϕ, θ) pairs are still spaced approximately uniformly. To emphasize this, the datapoints in the figures in Section V are centered at the actual measured location data rather than the locations corresponding to the intended angles. Though there are slight offsets from the grid of the "globe", the measured locations effectively cover the entire space.

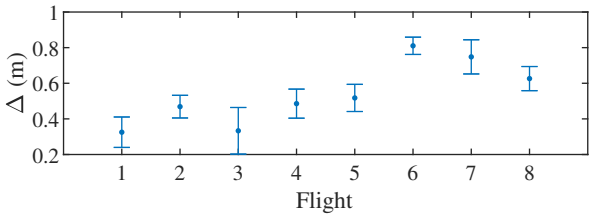

(a) Transmitter location displacement for each flight.

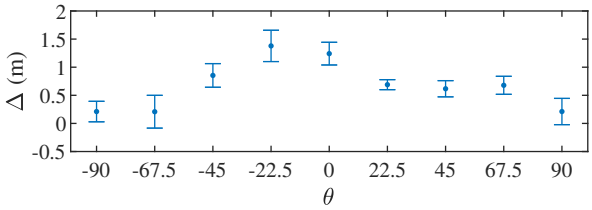

(b) Receiver location displacement for locations $(\phi = 0, \theta)$.

Fig. 4: Mean and standard deviation of (a) TX and (b) RX UAV position displacement from intended.

V. Effect of Position and Antenna Orientation on Capacity

We now demonstrate the effect of the combination of relative drone positioning and antenna orientation on the achievable capacity of the air-to-air channel and show that an antenna selection process can achieve optimal performance.

In the following "globe" figures, each datapoint corresponds to a measurement location described by a (ϕ, θ) pair. The location of the datapoint represents the actual location recorded during the experiment, whereas the grid/frame is the intended position. The size and color of each datapoint is proportional to the average capacity over 100 channel estimates at that (ϕ, θ) location.

A. Fixed Antenna Orientations

1) TXV-RXV: Fig. 5a shows the average capacity of each measurement location for half of the locations for the VV channel. Notice that the highest capacity values are achieved when the elevation angle is close to 0, i.e. "equator" of

the globe. Conversely, for the locations where the vertical displacement is high, i.e. elevation angles close to ± 90 or the "poles", the average capacity is much lower. There is less dependence on azimuth angle, as expected for a vertically oriented dipole antenna.

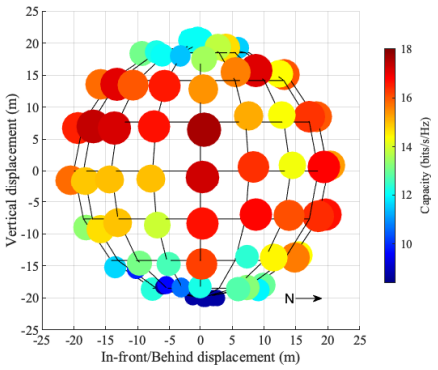

(a) VV

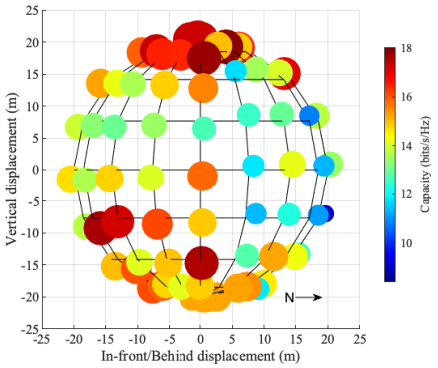

(b) HH

Fig. 5: Average capacity of the (a) VV and (b) HH TX-RX antenna pairs.

2) TXH-RXH: Now consider the capacities shown in Fig. 5b. As opposed to the VV channel, the highest capacities in the 3D space are found at elevation angles close to $\pm 90°$ (i.e. the "poles" of the globe), while the average capacities of the locations with elevation angle closer to 0 are lower.

The 3D picture for the VH and HV situations are similar but omitted for space constraints. There are many things that affect the channel in these situations: noise due to UAV motion and vibration, antenna cross- or co-polarization, mismatches or alignments of antenna radiation pattern, and signal blockages or enhancements due to the drone body at either the transmitter or receiver. The result, however, is that the channel has a strong co-dependence on both the relative position of each drone and the orientations of each antenna. Thus in applications where the position of the drones is arbitrary, if the on-board radios are equipped with a single, fixed antenna, the drone-to-drone channel might experience deep fades due only to the changes in relative position.

B. Best Antenna Pair

Fig. 6a shows the transmitter-receiver pair that achieves the highest average capacity at each measurement location. The same patterns as Fig. 5 are shown here as well: VV is best around $\theta = 0°$, HH is best around $\theta = \pm 90°$. There are several locations at intermediate elevation angles, however, where the average measured capacity of the cross-oriented antenna pairs, VH and HV, was the highest of all pairs.

One way to prevent the type of fading events described above could be to outfit both the transmitter and receiver drone with two antennas mounted vertically and horizontally. These antennas could each be connected to a single radio chain through a switch, or to their own radio chain. The transmitter and receiver could then optimally select which of the two antennas to use based on their relative position to one another. In Fig. 6b, each capacity datapoint is whichever was highest among the four transmitter-receiver pairs. Notice that the capacity is more or less constant near the highest value at all locations in the 3D space, i.e. we avoid the deep fades observed in the fixed VV or HH scenarios.

Fig. 6c shows box plots of the measured capacity over all locations which illustrates this result. The middle horizontal line represents the median measured capacity, while the dot shows the mean. The vertical bars depict the total range of the distribution. Outliers (marked with a "+") are values that lie outside 1.5 times the inter-quartile range (IQR), which is the difference between the 75th and 25th percentile. The median capacity over all locations in 3D space is over 16 bits/s/Hz which is better than any of the other four pairs, none of which are more than 15 bits/s/Hz; however, the real benefit is in the smaller variance. The IQR for the best antenna pair is 2.1 which indicates 50% of the locations were with 1 bits/s/Hz of the median value. The IQRs for the fixed VV, VH, HV, and HH pairs are 3.8, 4.0, 2.9 and 2.8 respectively indicating a larger spread of capacity values over the space. Moreover, the lowest capacity measured from the best antenna pair strategy was 12.4 bits/s/Hz while the fixed antenna pairs had much lower capacities at certain locations.

VI. Conclusion

In this paper, we presented an A2A measurement campaign which studied the effects of 3D relative positioning and antenna orientation on UAV networks. In the study, each UAV was outfitted with a vertical and a horizontally mounted antenna. We then measured the channel of four transmit-receive antenna orientation pairs (VV, VH, HV, and HH) at 114 unique locations in 3D space across various azimuth and elevation angles and a constant radial distance. We found that none of the four fixed pairs experience a better channel than others over all 3D space–each of them experiences the strongest channel at certain angles and experiences fading at others. Therefore, optimally selecting between two antennas at both the transmitter and receiver could result in a stronger and more consistent wireless performance over all angles in 3D space. This could allow UAVs to form arbitrary topologies in flight and maintain a consistent connection with one another.

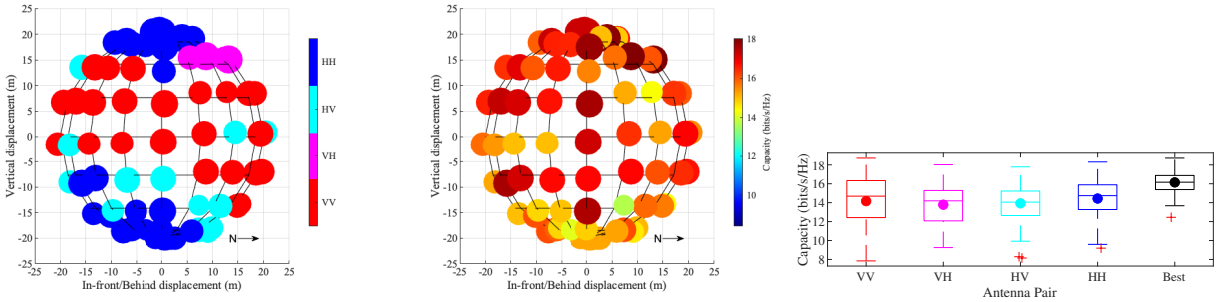

(a) Best TX-RX antenna pair. (b) Best pair capacity. (c) Distribution of capacity.

Fig. 6: Best performing TX-RX antenna pair (a) and its capacity (b). Distribution of measured capacity over 3D space of four fixed TX-RX pairs and "best-pair" selection strategy (c.)

ACKNOWLEDGMENTS

This work was in part supported by NSF grants CNS-1823304 and CNS-1909381 and Air Force Office of Scientific Research grant FA9550-19-1-0375.

REFERENCES

[1] A. Tahir, J. Böling, M.-H. Haghbayan, H. T. Toivonen, and J. Plosila, "Swarms of Unmanned Aerial Vehicles — A Survey," *Journal of Industrial Information Integration*, vol. 16, p. 100106, Dec. 2019. [Online]. Available: https://www.sciencedirect.com/science/article/pii/S2452414X18300086

[2] A. Mairaj, A. I. Baba, and A. Y. Javaid, "Application Specific Drone Simulators: Recent Advances and Challenges," *Simulation Modelling Practice and Theory*, vol. 94, pp. 100–117, Jul. 2019, arXiv: 1902.00616. [Online]. Available: http://arxiv.org/abs/1902.00616

[3] S. Baidya, Z. Shaikh, and M. Levorato, "FlyNetSim: An Open Source Synchronized UAV Network Simulator based on ns-3 and Ardupilot," in *Proceedings of the 21st ACM International Conference on Modeling, Analysis and Simulation of Wireless and Mobile Systems*, ser. MSWIM '18. New York, NY, USA: Association for Computing Machinery, Oct. 2018, pp. 37–45. [Online]. Available: https://doi.org/10.1145/3242102.3242118

[4] A. A. Khuwaja, Y. Chen, N. Zhao, M. Alouini, and P. Dobbins, "A Survey of Channel Modeling for UAV Communications," *IEEE Communications Surveys Tutorials*, vol. 20, no. 4, pp. 2804–2821, 2018.

[5] W. Khawaja, I. Guvenc, D. W. Matolak, U. Fiebig, and N. Schneckenburger, "A Survey of Air-to-Ground Propagation Channel Modeling for Unmanned Aerial Vehicles," *IEEE Communications Surveys Tutorials*, vol. 21, no. 3, pp. 2361–2391, 2019.

[6] R. Sun, D. W. Matolak, and W. Rayess, "Air-Ground Channel Characterization for Unmanned Aircraft Systems—Part IV: Airframe Shadowing," *IEEE Transactions on Vehicular Technology*, vol. 66, no. 9, pp. 7643–7652, Sep. 2017.

[7] J. Kunisch, I. d. l. Torre, A. Winkelmann, M. Eube, and T. Fuss, "Wideband time-variant air-to-ground radio channel measurements at 5 GHz," in *Proceedings of the 5th European Conference on Antennas and Propagation (EUCAP)*, Apr. 2011, pp. 1386–1390, iSSN: 2164-3342.

[8] J. Chen, D. Raye, W. Khawaja, P. Sinha, and I. Guvenc, "Impact of 3D UWB Antenna Radiation Pattern on Air-to-Ground Drone Connectivity," in *2018 IEEE 88th Vehicular Technology Conference (VTC-Fall)*, Aug. 2018, pp. 1–5, iSSN: 2577-2465.

[9] W. Khawaja, O. Ozdemir, F. Erden, I. Guvenc, and D. W. Matolak, "UWB Air-to-Ground Propagation Channel Measurements and Modeling Using UAVs," in *2019 IEEE Aerospace Conference*, Mar. 2019, pp. 1–10, iSSN: 1095-323X.

[10] W. Khawaja, O. Ozdemir, and I. Guvenc, "Temporal and Spatial Characteristics of mm Wave Propagation Channels for UAVs," in *2018 11th Global Symposium on Millimeter Waves (GSMM)*, May 2018, pp. 1–6.

[11] ——, "UAV Air-to-Ground Channel Characterization for mmWave Systems," in *2017 IEEE 86th Vehicular Technology Conference (VTC-Fall)*, Sep. 2017, pp. 1–5.

[12] J. Romeu, A. Aguasca, J. Alonso, S. Blanch, and R. R. Martins, "Small UAV radiocommunication channel characterization," in *Proceedings of the Fourth European Conference on Antennas and Propagation*, Apr. 2010, pp. 1–5, iSSN: 2164-3342.

[13] T. Tavares, P. Sebastião, N. Souto, F. J. Velez, F. Cercas, M. Ribeiro, and A. Correia, "Generalized LUI Propagation Model for UAVs Communications Using Terrestrial Cellular Networks," in *2015 IEEE 82nd Vehicular Technology Conference (VTC2015-Fall)*, Sep. 2015, pp. 1–6.

[14] C. Cheng, P. Hsiao, H. T. Kung, and D. Vlah, "Performance Measurement of 802.11a Wireless Links from UAV to Ground Nodes with Various Antenna Orientations," in *Proceedings of 15th International Conference on Computer Communications and Networks*, Oct. 2006, pp. 303–308, iSSN: 1095-2055.

[15] E. Yanmaz, R. Kuschnig, and C. Bettstetter, "Channel measurements over 802.11a-based UAV-to-ground links," in *2011 IEEE GLOBECOM Workshops (GC Wkshps)*, Dec. 2011, pp. 1280–1284, iSSN: 2166-0077.

[16] ——, "Achieving air-ground communications in 802.11 networks with three-dimensional aerial mobility," in *2013 Proceedings IEEE INFOCOM*, Apr. 2013, pp. 120–124, iSSN: 0743-166X.

[17] N. Ahmed, S. S. Kanhere, and S. Jha, "On the importance of link characterization for aerial wireless sensor networks," *IEEE Communications Magazine*, vol. 54, no. 5, pp. 52–57, May 2016.

[18] J. Allred, A. B. Hasan, S. Panichsakul, W. Pisano, P. Gray, J. Huang, R. Han, D. Lawrence, and K. Mohseni, "SensorFlock: an airborne wireless sensor network of micro-air vehicles," in *Proceedings of the 5th international conference on Embedded networked sensor systems*, ser. SenSys '07. New York, NY, USA: Association for Computing Machinery, Nov. 2007, pp. 117–129. [Online]. Available: https://doi.org/10.1145/1322263.1322275

[19] A. Shaw and K. Mohseni, "A Fluid Dynamic Based Coordination of a Wireless Sensor Network of Unmanned Aerial Vehicles: 3-D Simulation and Wireless Communication Characterization," *IEEE Sensors Journal*, vol. 11, no. 3, pp. 722–736, Mar. 2011.

[20] N. Goddemeier and C. Wietfeld, "Investigation of Air-to-Air Channel Characteristics and a UAV Specific Extension to the Rice Model," in *2015 IEEE Globecom Workshops (GC Wkshps)*. San Diego, CA, USA: IEEE, Dec. 2015, pp. 1–5. [Online]. Available: http://ieeexplore.ieee.org/document/7414180/

[21] M. Badi, J. Wensowitch, D. Rajan, and J. Camp, "Experimental Evaluation of Antenna Polarization and Elevation Effects on Drone Communications," in *Proceedings of the 22nd International ACM Conference on Modeling, Analysis and Simulation of Wireless and Mobile Systems*, ser. MSWIM '19. New York, NY, USA: Association for Computing Machinery, Nov. 2019, pp. 211–220. [Online]. Available: https://doi.org/10.1145/3345768.3355916

[22] ——, "Experimentally Analyzing Diverse Antenna Placements and Orientations for UAV Communications," *IEEE Transactions on Vehicular Technology*, vol. 69, no. 12, pp. 14 989–15 004, Dec. 2020.

[23] D. Tse and P. Viswanath, *Fundamentals of Wireless Communication*, 1st ed. Cambridge University Press, May 2005. [Online]. Available: https://www.cambridge.org/core/product/identifier/9780511807213/type/book